



Cite this: *Chem. Commun.*, 2022, 58, 13278

Received 30th August 2022,
Accepted 27th October 2022

DOI: 10.1039/d2cc04803e

rsc.li/chemcomm

Isostructural σ -hydrocarbyl phospholide complexes of uranium, neptunium, and plutonium†‡

Michaela Černá,^a John A. Seed,^{ib} Sara Garrido Fernandez,^a Michael T. Janicke,^b Brian L. Scott,^{ib} George F. S. Whitehead,^{ib} Andrew J. Gaunt^{ib} and Conrad A. P. Goodwin^{ib}*^{ab}

σ -Hydrocarbyl complexes of the form $[M(\eta^5\text{-PC}_4\text{Me}_4)_2(\mu\text{-}\eta^1\text{-}\eta^6\text{-CH}_2\text{Ph})_2K(\eta^6\text{-arene})]$ ($M = \text{La, Ce, Pr, U, Np, Pu}$; arene = benzene or toluene) were synthesised in one-pot reactions from $[M]_3(\text{THF})_4$, or $[U(\text{BH}_4)_3(\text{toluene})]$ ($M = \text{U}$). All complexes were examined by multinuclear (^1H , $^{13}\text{C}\{^1\text{H}\}$, $^{31}\text{P}\{^1\text{H}\}$) NMR and UV-vis-NIR spectroscopy, as well as single-crystal X-ray diffraction from which molecular metal–phosphorus bonds for Np and Pu, and a σ -hydrocarbyl metal–carbon bond for Pu, have been structurally authenticated.

σ -Hydrocarbyl complexes are an important class of molecule for their numerous roles in both catalysis and fundamental bond formation reactions across the periodic table. While the close energetic matching and spatial overlap of metal and carbon orbitals affords facile redox chemistry in noble metal catalytic processes, poor matching in rare-earth and actinide hydrocarbyl complexes results in highly polar linkages amenable to protonolysis and bond-metathesis chemistry.¹

Protonolysis reactions using basic hydrocarbyl groups in U^{IV} and Th^{IV} molecules have proven invaluable for the isolation of diverse metal–element linkages such as imido-, phosphido-, phosphinidene-, alkylidene-, hydrides, and others.² Thus, their utility in facilitating the comparison of An^{IV} ($\text{An} = \text{Th, U}$) covalency through the examination of metal–element multiple bonds is patent. Hydrocarbyls also serve as precursors, *via* hydrogenolysis with H_2 ,³ or with silanes,⁴ to molecular

metal-hydrides for which no transuranium examples have been reported. Attempts to extend tetravalent metal-hydrocarbyl chemistry to the next actinide element, Np, have proven non-trivial, in part because reduction of Np^{IV} precursors to Np^{III} is facile due to the readily accessible $\text{Np}^{\text{IV/III}}$ redox couple (*ca.* +0.147 to +0.218 V *vs.* NHE).⁵ This complication is likely to extend to many of the transuranium elements for which the trivalent oxidation state is the most prevalent. Conversely, the increasing accessibility of An^{III} with higher Z elements can enable direct comparison to Ln^{III} bonding, and hence insight into the comparative role of 4f or 5f electrons in bonding. Trivalent σ -hydrocarbyl complexes, which can be isolated using the small (milligram) reaction scales commonly employed for transuranium research, can help in providing access to new 4f *vs.* 5f bonding comparisons.

Here we show that a per-alkylated phospholide, TMP ($\text{TMP} = \{\text{PC}_4\text{Me}_4\}$) allows the one-pot synthesis and isolation of trivalent dibenzyl-ate complexes of the form $[M(\text{TMP})_2(\mu\text{-}\eta^1\text{-}\eta^6\text{-C}_7\text{H}_7)_2K(\eta^6\text{-arene})]$ (arene = toluene or benzene) of U, Np, and Pu, along with isoradial lanthanide congeners La, Ce, and Pr. The Np and Pu complexes herein represent unique examples of M–P bonds for these elements, and complexation with a carbocyclic ligand other than cyclopentadienide or cyclooctatetraenide. The Pu complex is a rare example of a structurally characterised Pu σ -hydrocarbyl.

Previous reports have shown that salt occlusion and oligomerisation reactions plague trivalent rare earth and f-block phospholide chemistry.⁶ The facile isolation of $[\text{U}^{\text{III}}(\text{TMP})(\mu\text{-}\eta^1\text{-}\eta^6\text{-TMP})(\text{BH}_4)_2]$ ($\text{TMP} = \{\text{PC}_4\text{Me}_4\}$) by reduction of $[\text{U}^{\text{IV}}(\text{TMP})_2(\text{BH}_4)_2]$ suggested that a suitable tetravalent precursor might allow, through a subsequent reduction step, access to discrete heteroleptic Np^{III} molecules with which to synthesise σ -hydrocarbyl complexes.⁷ As $[\text{U}^{\text{IV}}(\text{TMP})_3(\text{Cl})]$ is known,⁸ and $[\text{Np}^{\text{IV}}\text{Cl}_4(\text{DME})_2]$ is a readily synthesised precursor,⁹ it seemed reasonable to target $[\text{Np}^{\text{IV}}(\text{TMP})_3(\text{Cl})]$ first to help identify differences in the chemistries of Np/U using a model system. The reaction between $[\text{Np}^{\text{IV}}\text{Cl}_4(\text{DME})_2]$ and 3 equivalents of KTMP in Et_2O or THF led to the isolation of several crystals of the Np^{III} bis-TMP complexes 1

^a Centre for Radiochemistry Research, Department of Chemistry, The University of Manchester, Oxford Road, Manchester, M13 9PL, UK.

E-mail: conrad.goodwin@manchester.ac.uk

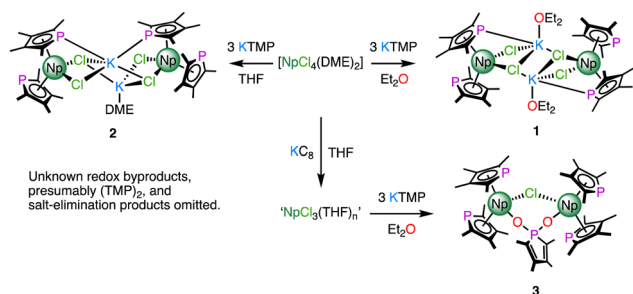
^b Chemistry Division, Los Alamos National Laboratory, Los Alamos, New Mexico, 87545, USA

^c Materials Physics & Applications Division, Los Alamos National Laboratory, Los Alamos, New Mexico, 87545, USA

† Research data files supporting this work are available from Figshare at DOI: <https://doi.org/10.48420/20390763>.

‡ Electronic supplementary information (ESI) available. CCDC 2193335–2193346, 2202840. For ESI and crystallographic data in CIF or other electronic format see DOI: <https://doi.org/10.1039/d2cc04803e>



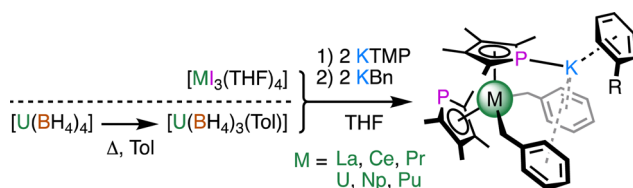
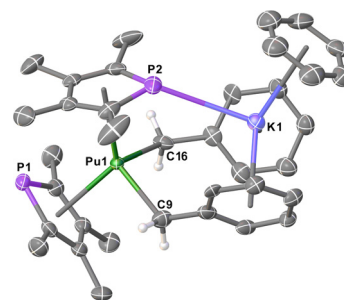
Scheme 1 Syntheses of complexes **1–3**.

and **2** respectively (Scheme 1). On one occasion, the use of a trivalent precursor, $\text{Np}^{\text{III}}\text{Cl}_3(\text{THF})_n$ prepared *in situ*,¹⁰ afforded several crystals of dinuclear complex, **3**. Complexes **1** and **3** could not be separated from impurities such as $[\text{K}(\text{THF})_2(\eta^5\text{-TMP})]_n$ (**4**) – see ESI† for structural details of **1–4**, and UV-vis-NIR and multinuclear NMR spectroscopy of **2**.

Next, we turned to $[\text{Ml}_3(\text{THF})_4]$ ($\text{M} = \text{La}, \text{Ce}, \text{Pr}, \text{U}, \text{Np}, \text{Pu}$) as well-defined trivalent precursors. The micromole-scale (35 mg) reaction in THF between $[\text{U}_3(\text{THF})_4]$ (prepared *in situ* from $\text{U}_3(\text{OEt}_2)_x$) and 2 equivalents of KTMP gave a dark green reaction mixture, a small portion of which gave several crystals of $[\text{U}(\text{TMP})_2(\text{I})(\text{THF})]$ (**5**). Addition of 2 equivalents of KBn (Bn = benzyl) to the remaining THF solution followed by workup (see ESI†) gave several crystals of $[\text{U}(\text{TMP})_2(\mu\text{-}\eta^1\text{-C}_7\text{H}_7)_2\text{K}(\eta^6\text{-C}_6\text{H}_6)]$ (**7U**).

Separate reactions using $[\text{Ml}_3(\text{THF})_4]$ with 2 equivalents of KTMP and 2 equivalents of KBn in THF at -98°C or room temperature, followed by extraction and crystallisation from boiling toluene gave the isomorphous series $[\text{M}(\text{TMP})_2(\mu\text{-}\eta^1\text{-C}_7\text{H}_7)_2\text{K}(\eta^6\text{-C}_7\text{H}_8)]$ (**6M**, $\text{M} = \text{La}, \text{Ce}, \text{Pr}, \text{Np}, \text{Pu}$; Scheme 2) in low to moderate yield (16%, Pu to 53%, Pr). These metals were chosen based on the similarities of their ionic radii, *e.g.* U^{III} and La^{III} (1.025 Å vs. 1.032 Å).¹¹ Complex **6U** was synthesised on a preparative scale (0.5 mmol) from $[\text{U}(\text{BH}_4)_3(\text{toluene})]$ ¹² in modest yield (29%). Recrystallisation of several mg each of **6U**, **6Np**, and **6Pu** from boiling benzene gave $[\text{M}(\text{TMP})_2(\mu\text{-}\eta^1\text{-C}_7\text{H}_7)_2\text{K}(\eta^6\text{-C}_6\text{H}_6)]$ (**7M**), which allowed us to examine the influence of the arene on the structure.

All **6M** complexes crystallised in the non-centrosymmetric space group $Pna2_1$ with one molecule in the asymmetric unit, whereas **7M** crystallised in the centrosymmetric space group $Pnma$ with half a molecule in the asymmetric unit. The structure of **7Pu** is shown in Fig. 1 (see ESI† for others) which features a bis- η^5 -TMP wedge-shaped arrangement

Scheme 2 Synthesis of complexes **6M** ($\text{R} = \text{Me}$; $\text{M} = \text{La}, \text{Ce}, \text{Pr}, \text{U}, \text{Np}, \text{Pu}$) and **7M** ($\text{R} = \text{H}$, $\text{M} = \text{U}, \text{Np}, \text{Pu}$).Fig. 1 Molecular structure of $[\text{Pu}(\text{TMP})_2\text{Bn}_2\text{K}(\text{benzene})]$ **7Pu**. Ellipsoids set at 50% probability and H-atoms (except on C9 and C16) removed for clarity.

($\text{Pu1-P1} = 2.9533(13)$ Å, $\text{Pu1}\cdots\text{TMP}_{\text{cent}} = 2.5931(15)$ Å; $\text{Pu1-P2} = 2.9816(14)$ Å, $\text{Pu1}\cdots\text{TMP}_{\text{cent}} = 2.5821(14)$ Å; $\text{TMP}_{\text{cent}}\cdots\text{Pu1}\cdots\text{TMP}_{\text{cent}} = 127.56(5)^\circ$). In **7Pu** both benzyl groups are bound η^1 to the Pu-atom ($\text{Pu1-C9} = 2.542(19)$ Å; $\text{Pu1-C16} = 2.614(19)$ Å; $\text{C9-Pu1-C16} = 107.1(4)^\circ$), these Pu-C lengths are unremarkable when compared to known U^{III} mono- and bis-benzyl complexes,¹³ and accounting for the difference in their between 6-coordinate U^{III} (1.025 Å) and Pu^{III} (1.00 Å).¹¹ The K-atom is bound η^6 to the C₆ rings from both benzyl groups ($\text{Bn}_{\text{cent}}\cdots\text{K1} = 2.875(11)$ and $2.948(10)$ Å; $\text{Bn}_{\text{cent}}\cdots\text{K1}\cdots\text{Bn}_{\text{cent}} = 113.8(3)^\circ$) along with an η^6 -benzene molecule, and a P-K contact ($3.3270(18)$ Å) with one of the TMP rings. Bond lengths and angles for **6M** and **7M** complexes are summarised in Table 1 (data for **6Pu** is not of sufficient quality for discussion). A homoleptic Pu hydrocarbyl complex has been synthesised previously, $[\text{Pu}\{\text{CH}(\text{SiMe}_3)_2\}_3]$, though structural data is not available for comparison.¹⁴

Table 1 shows the arene coordinating to K1 has a small impact on the overall structure. The M-P, K-P, and $\text{M}\cdots\text{TMP}_{\text{cent}}$ lengths all shorten somewhat upon switching from toluene to benzene, and the M-C_{Bn} bond lengths become less equivalent. For example, the difference between the Np-C_{Bn} bonds in **6Np** is 0.05(2) Å which is statistically indistinguishable (3σ criteria), but it is 0.12(2) Å for **7Np** which shows the two bonds are distinct. This is presumably due to packing differences of the $\{(\eta^6\text{-Bn})_2\text{K}(\text{arene})\}$ unit in **6M** and **7M**. Metrical parameters for the series change broadly as expected with the ionic radii of the metals. Equivalent M-P and M-C bond lengths decrease on average from La to Pr, and from U to Pu. However, within the **7M** series, **7Np** displays noticeably shorter M-P bonds and $\text{M}\cdots\text{TMP}_{\text{cent}}$ distances than **7Pu** (though the M-C_{Bn} distances overlap slightly within the 3σ criteria). This is not the first time Np complexes have been shown to be outliers.^{9a} As is commonly seen, actinide **6M** or **7M** have bond lengths that are shorter than corresponding lanthanide complexes by an amount larger than the difference in their ionic radii. For example: the differences between the two unique M-P bond lengths in **6La** and **6U** are 0.068(16) Å (M-P1) and 0.064(2) Å (M-P2), which is larger than the difference in their radii (0.007 Å). This discrepancy decreases as the series is traversed.^{9a,15}

¹H NMR spectroscopy of diamagnetic **6La** in $\text{C}_4\text{D}_8\text{O}$ or C_6D_6 reveal spectra consistent with C_2 symmetry in solution. The

Table 1 Summary of bond lengths and angles for **6M** (M = La, Ce, Pr, U, Np) and **7M** (M = U, Np, Pu)

	M–P (Å)	M–C _{Bn} (Å)	M···TMP _{cent} (Å)	K–P (Å)	TMP _{cent} ···M···TMP _{cent} (°)
6M					
La	3.0112(12) 3.0407(15)	2.622(8) 2.675(9)	2.650(4) 2.635(4)	3.323(2)	127.63(12)
U	2.9432(11) 2.9766(14)	2.577(7) 2.597(7)	2.580(3) 2.564(3)	3.303(2)	128.33(11)
Ce	2.9863(14) 3.0197(16)	2.619(8) 2.631(10)	2.623(3) 2.609(4)	3.313(2)	127.59(11)
Np	2.940(2) 2.971(3)	2.519(18) 2.573(15)	2.577(9) 2.564(8)	3.317(4)	127.8(3)
Pr	2.9672(9) 3.0034(11)	2.592(6) 2.598(5)	2.606(2) 2.593(2)	3.3118(16)	128.07(8)
7M					
U	2.9576(11) 2.9857(11)	2.556(17) 2.654(16)	2.5915(2) 2.5816(11)	3.3275(15)	127.624(9)
Np	2.9147(11) 2.9403(12)	2.479(17) 2.603(16)	2.5547(12) 2.5484(12)	3.2805(16)	127.12(4)
Pu	2.9533(13) 2.9816(14)	2.542(19) 2.614(19)	2.5931(15) 2.5821(14)	3.3270(18)	127.56(5)

TMP 3,4-Me shows a singlet at 1.96 ppm, and the 2,5-Me peak at 2.8 ppm is split ($^3J_{\text{HP}} = 9.6$ Hz) due to coupling with ^{31}P (100% $I = 1/2$). Resonances for the benzyl groups were well resolved as triplets at 6.67 ppm (*m*) and 6.14 ppm (*p*), a doublet at 6.40 ppm (*o*), and a singlet at 1.04 ppm for the benzylic protons. Benzyl CH_2 protons were located in the ^1H NMR spectra of all paramagnetic **6M** complexes (**6Ce**, 1.22 ppm; **6Pr**, 7.48 ppm; **6U**, –55.31 ppm; **6Np**, –60.30 ppm; **6Pu**, –18.75 ppm). In all except **6Pu** we could definitively assign all unique CH groups for the benzyl moiety (see ESI†). The $^{13}\text{C}\{^1\text{H}\}$ NMR spectrum of **6La** revealed doublets at 15.32 and 16.34 ppm ($^3J_{\text{CP}} = 5.3$ and 28.9 Hz) for the TMP methyl groups due to ^{13}C – ^{31}P coupling; and the corresponding ring carbons at 135.95 and 142.82 ppm also presented as doublets ($^3J_{\text{CP}} = 2.0$ and 41.2 Hz). $^{13}\text{C}\{^1\text{H}\}$ NMR spectroscopy was uninformative for all other complexes. The $^{31}\text{P}\{^1\text{H}\}$ NMR spectrum of **6La** showed a singlet at 98.28 ppm (*cf.* KTMP 74.32 ppm in $\text{C}_4\text{H}_8\text{O}/\text{C}_6\text{D}_6$ – see ESI†), consistent with C_2 symmetry in solution. Paramagnetic **6M** complexes displayed a broad range of ^{31}P chemical shifts (**6Ce**, 175.3 ppm; **6Pr**, 293.5 ppm; **6U**, 738.8 ppm; **6Np**, –497.9 ppm). We could not unambiguously locate the TMP ^{31}P peak for **6Pu** (see ESI†).

UV-vis-NIR spectra of **6M** (M = La, Ce, Pr) show a broad ligand-to-metal charge-transfer (LMCT) band that tails in from the edge of the spectral range to *ca.* 22 000 cm^{-1} . This is responsible for the red-orange colour of all of these complexes, and is the only feature for **6La**; whereas **6Ce** shows a broad feature at *ca.* 20 800 cm^{-1} ($\epsilon = 317 \text{ M}^{-1} \text{ cm}^{-1}$) for a symmetry allowed $4f \rightarrow 5d$ transition; and **6Pr** shows numerous weak $4f \rightarrow 4f$ peaks from 6000–20 000 cm^{-1} ($\epsilon = 10$ –52 $\text{M}^{-1} \text{ cm}^{-1}$), while a shoulder at 21 622 cm^{-1} ($\epsilon = 145 \text{ M}^{-1} \text{ cm}^{-1}$) is plausibly due to the $^1\text{S}_0$ excitation.¹⁶ The spectra of **6Np** and **6Pu** feature multiple weak peaks between 6000–14 000 cm^{-1} ($\epsilon = 16$ –100 $\text{M}^{-1} \text{ cm}^{-1}$) which are characteristic of $5f \rightarrow 5f$ transitions. For **6U**, this region is broad, mostly featureless, and with modest absorption ($\epsilon = 200$ –550 $\text{M}^{-1} \text{ cm}^{-1}$) – see Fig. 2. Comparatively strong features which tail into the visible region at *ca.* 12 000 and 19 000 cm^{-1} for **6U** ($\epsilon = 550$ and 1100 $\text{M}^{-1} \text{ cm}^{-1}$

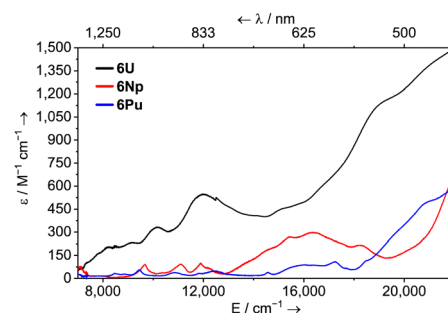


Fig. 2 UV-vis-NIR spectra of [U(TMP)₂Bn₂K(toluene)] (**6U**, black line) in THF (0.97 mM), and [Np(TMP)₂Bn₂K(toluene)] (**6Np**, red line) in toluene (0.50 mM), and [Pu(TMP)₂Bn₂K(toluene)] (**6Pu**, blue line) in toluene (1.00 mM) between 7000–22 000 cm^{-1} (1429–455 nm) at room temperature.

respectively); 16 400 cm^{-1} for **6Np** ($\epsilon = 300 \text{ M}^{-1} \text{ cm}^{-1}$); and *ca.* 17 200 and 22 000 cm^{-1} for **6Pu** ($\epsilon = 108$ and 614 $\text{M}^{-1} \text{ cm}^{-1}$ respectively) are responsible for the dark green/brown (**6U**), apple green (**6Np**), and golden-brown (**6Pu**) colours. These excitations are likely too low in energy for $5f \rightarrow 6d$ transitions, though have absorptivities somewhat high for typical $5f \rightarrow 5f$ transitions. One possible cause for this is an intensity-stealing mechanism by mixing of $5f$ states with a charge-transfer or intra-ligand transition of different parity which has previously been invoked to explain similar observations.¹⁷ It is noteworthy that the transitions between 14 000–22 000 cm^{-1} for **6Pu** are *ca.* 5 to 10 times more intense than several other Pu^{III} complexes with reported ϵ values.^{9a,18}

The U^{III} assignment of **6U** was confirmed by SQUID magnetometry (Fig. 3). A powdered sample exhibits slow reduction in μ_{eff} (χT) across the entire temperature range from 2.75 μ_{B} (0.95 $\text{cm}^3 \text{ K mol}^{-1}$) at 300 K to a minimum of 1.71 μ_{B} (0.36 $\text{cm}^3 \text{ K mol}^{-1}$) at 1.8 K, which is consistent with gradual thermal depopulation of excited crystal field states of the split $^4\text{I}_{9/2}$ ground multiplet, and is typical for U^{III} complexes.¹⁹ The magnetisation at 2 K saturates to a value of 0.89 $\mu_{\text{B}} \text{ mol}^{-1}$ at 7 T



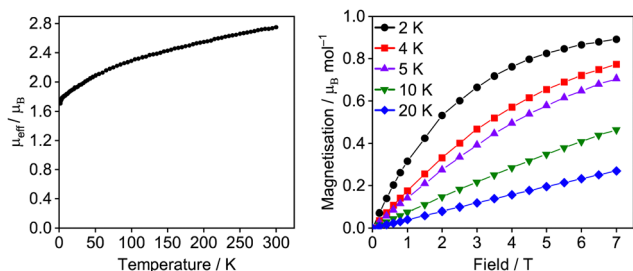


Fig. 3 Variable-temperature effective magnetic moment ($\mu_{\text{eff}}/\mu_{\text{B}}$) versus temperature for **6U** at 0.5 T and variable-field molar magnetisation for **6U**.

which is also in agreement with a U^{III} assignment for **6U**. Variable field and temperature magnetometry was also performed on **6Ce** and **6Pr** which displayed μ_{eff} values of $2.16 \mu_{\text{B}}$ and $3.24 \mu_{\text{B}}$ respectively at 300 K, comparing well with free-ion values for $^2F_{5/2}$ and 3H_4 ground states. Their low temperature μ_{eff} values and saturation properties are unremarkable (see ESI†).²⁰

We have prepared a range of f-block bis-per-alkylated phospholide complexes from La–Pr, and U–Pu, and shown that this framework is able to support the isolation and characterisation of isomorphous bis-benzyl-potassium salts. Despite these compounds containing paramagnetic ions (except La), we were able to observe ^{31}P NMR chemical shifts from the phospholide ligands with all metals except Pu. In future, this could be leveraged for *in situ* monitoring of protonolysis reactions with Np and Pu by NMR spectroscopy – elements for which macro-scale chemistry is not routinely possible in most laboratories.

Transuranium work was conducted at Los Alamos National Laboratory (LANL). AJG and BLS acknowledge the U.S. Department of Energy, Office of Science, Office of Basic Energy Sciences, Chemical Sciences, Geosciences, and Biosciences Division, Heavy Element Chemistry Program at LANL (DE-AC52-06NA25396). CAPG was sponsored by a Distinguished J. R. Oppenheimer Postdoctoral Fellowship (LANL-LDRD, 20180703PRD1). For work at the University of Manchester (UoM) we thank the Royal Society (URF\R1\211271 to CAPG); and the UoM (Research Bursary to SGF). We acknowledge funding from the EPSRC (EP/K039547/1 and EP/P001386/1 for NMR spectroscopy and X-ray diffraction), and the EPSRC UK National Electron Paramagnetic Resonance Service for SQUID magnetometer access (EP/S033181/1). We thank Prof. Stephen Liddle for support (JAS). Elemental Analyses were performed at the UoM by Mr Martin Jennings and Ms Anne Davies.

Conflicts of interest

There are no conflicts to declare.

References

- 1 C. E. Housecroft and A. G. Sharpe, *Inorganic Chemistry*, Prentice Hall, Pearson, 2008.
- 2 (a) D. S. J. Arney and C. J. Burns, *J. Am. Chem. Soc.*, 1995, **117**, 9448–9460; (b) D. S. J. Arney, R. C. Schnabel, B. C. Scott and C. J. Burns, *J. Am. Chem. Soc.*, 1996, **118**, 6780–6781; (c) A. J. Wooles, D. P. Mills, W. Lewis, A. J. Blake and S. T. Liddle, *Dalton Trans.*, 2010, 500–510;
- (d) T. W. Hayton, *Chem. Commun.*, 2013, **49**, 2956–2973;
- (e) J. K. Pagano, J. M. Dorhout, K. R. Czerwinski, D. E. Morris, B. L. Scott, R. Waterman and J. L. Kiplinger, *Organometallics*, 2016, **35**, 617–620; (f) E. P. Wildman, G. Balázs, A. J. Wooles, M. Scheer and S. T. Liddle, *Nat. Commun.*, 2016, **7**, 12884.
- 3 P. J. Fagan, J. M. Manriquez, T. J. Marks, C. S. Day, S. H. Vollmer and V. W. Day, *Organometallics*, 1982, **1**, 170–180.
- 4 J. K. Pagano, J. M. Dorhout, R. Waterman, K. R. Czerwinski and J. L. Kiplinger, *Chem. Commun.*, 2015, **51**, 17379–17381.
- 5 (a) S. Kihara, Z. Yoshida, H. Aoyagi, K. Maeda, O. Shirai, Y. Kitatsuiji and Y. Yoshida, *Pure Appl. Chem.*, 1999, **71**, 1771–1807; (b) A. J. Myers, M. L. Tarlton, S. P. Kelley, W. W. Lukens and J. R. Walensky, *Angew. Chem., Int. Ed.*, 2019, **58**, 14891–14895; (c) D. C. Sonnenberger and J. G. Gaudiello, *Inorg. Chem.*, 1988, **27**, 2747–2748.
- 6 (a) F. Nief, P. Riant, L. Ricard, P. Desmurs and D. Baudry-Barbier, *Eur. J. Inorg. Chem.*, 1999, 1041–1045; (b) H.-J. Gosink, F. Nief, L. Ricard and F. Mathey, *Inorg. Chem.*, 2002, **34**, 1306–1307; (c) J. Liu, L. E. Nodarak, P. J. Cobb, M. J. Giansiracusa, F. Ortu, F. Tuna and D. P. Mills, *Dalton Trans.*, 2020, **49**, 6504–6511.
- 7 P. Gradoz, M. Ephritikhine, M. Lance, J. Vigner and M. Nierlich, *J. Organomet. Chem.*, 1994, **481**, 69–73.
- 8 A. Elkechai, Y. Mani, A. Boucekkine and M. Ephritikhine, *Inorg. Chem.*, 2012, **51**, 6943–6952.
- 9 (a) C. A. P. Goodwin, M. T. Janicke, B. L. Scott and A. J. Gaunt, *J. Am. Chem. Soc.*, 2021, **143**, 20680–20696; (b) S. D. Reilly, J. L. Brown, B. L. Scott and A. J. Gaunt, *Dalton Trans.*, 2014, **43**, 1498–1501.
- 10 S. A. Pattenau, N. H. Anderson, S. C. Bart, A. J. Gaunt and B. L. Scott, *Chem. Commun.*, 2018, **54**, 6113–6116.
- 11 R. D. Shannon, *Acta Crystallogr., Sect. A: Cryst. Phys., Diff., Theor. Gen. Crystallogr.*, 1976, **32**, 751–767.
- 12 T. V. Fetrow, J. P. Grabow, J. Leddy and S. R. Daly, *Inorg. Chem.*, 2021, **60**, 7593–7601.
- 13 D. Perales, R. Bhowmick, M. Zeller, P. Miro, B. Vlaisavljevich and S. C. Bart, *Chem. Commun.*, 2022, **58**, 9630–9633.
- 14 B. D. Zwick, A. P. Sattelberger and L. R. Avens, in *Transuranium Elements: A Half Century*, ed., L. R. Morss and J. Fuger, American Chemical Society, Washington DC, 1992, ch. 25, pp. 239–246.
- 15 (a) A. J. Gaunt, S. D. Reilly, A. E. Enriquez, B. L. Scott, J. A. Ibers, P. Sekar, K. I. Ingram, N. Kaltsoyannis and M. P. Neu, *Inorg. Chem.*, 2008, **47**, 29–41; (b) M. B. Jones and A. J. Gaunt, *Inorg. Rev.*, 2013, **113**, 1137–1198; (c) M. B. Jones, A. J. Gaunt, J. C. Gordon, N. Kaltsoyannis, M. P. Neu and B. L. Scott, *Chem. Sci.*, 2013, **4**, 1189–1203; (d) J. A. Macor, J. L. Brown, J. N. Cross, S. R. Daly, A. J. Gaunt, G. S. Girolami, M. T. Janicke, S. A. Kozimor, M. P. Neu, A. C. Olson, S. D. Reilly and B. L. Scott, *Dalton Trans.*, 2015, **44**, 18923–18936; (e) C. A. P. Goodwin, A. W. Schlingens, T. E. Albrecht-Schönart, E. R. Batista, A. Gaunt, M. T. Janicke, S. A. Kozimor, B. L. Scott, L. M. Stevens, F. D. White and P. Yang, *Angew. Chem., Int. Ed.*, 2021, **60**, 9459–9466; (f) S. E. Gilson and P. C. Burns, *Coord. Chem. Rev.*, 2021, **445**, 213994.
- 16 W. A. Hargreaves, *J. Condens. Matter Phys.*, 1992, **4**, 6141–6154.
- 17 (a) D. E. Morris, R. E. Da Re, K. C. Jantunen, I. Castro-Rodriguez and J. L. Kiplinger, *Organometallics*, 2004, **23**, 5142–5153; (b) E. M. Matson, W. P. Forrest, P. E. Fanwick and S. C. Bart, *Organometallics*, 2013, **32**, 1484–1492.
- 18 (a) L. R. Avens, S. G. Bott, D. L. Clark, A. P. Sattelberger, J. G. Watkin and B. D. Zwick, *Inorg. Chem.*, 1994, **33**, 2248–2256; (b) C. J. Windorff, G. P. Chen, J. N. Cross, W. J. Evans, F. Furche, A. J. Gaunt, M. T. Janicke, S. A. Kozimor and B. L. Scott, *J. Am. Chem. Soc.*, 2017, **139**, 3970–3973; (c) C. J. Windorff, J. M. Sperling, T. E. Albrecht-Schönart, Z. Bai, W. J. Evans, A. N. Gaiser, A. J. Gaunt, C. A. P. Goodwin, D. E. Hobart, Z. K. Huffman, D. N. Huh, B. E. Klamm, T. N. Poe and E. Warzecha, *Inorg. Chem.*, 2020, **59**, 13301–13314; (d) C. A. P. Goodwin, S. R. Ciccone, S. Bekoe, S. Majumdar, B. L. Scott, J. W. Ziller, A. J. Gaunt, F. Furche and W. J. Evans, *Chem. Commun.*, 2022, **58**, 997–1000.
- 19 (a) F. Moro, D. P. Mills, S. T. Liddle and J. van Slageren, *Angew. Chem., Int. Ed.*, 2013, **52**, 3430–3433; (b) D. R. Kindra and W. J. Evans, *Chem. Rev.*, 2014, **114**, 8865–8882.
- 20 (a) J. A. Seed, L. Vondung, F. Barton, A. J. Wooles, E. Lu, M. Gregson, R. W. Adams and S. T. Liddle, *Chem. – Eur. J.*, 2022, **28**, e202200761; (b) G. Balázs, F. G. N. Cloke, J. C. Green, R. M. Harker, A. Harrison, P. B. Hitchcock, C. N. Jardine and R. Walton, *Organometallics*, 2007, **26**, 3111–3119.

